Electronic Supplementary Information (ESI)

1. Preparation of the bio-oil, its composition and its main physical chemical features

Bio-oil was produced by the fast pyrolysis of biomass in a circulating fluidized bed with a capacity of 120 kg/h of oil at our Lab. The pyrolysis of biomass to produce bio-oil generally run from 520 to 540 ^{o}C (heating rate: about 10^4 ^{o}C/s, residence time: < 2 s), followed by a fast cooling process. Main products of the fast pyrolysis of biomass consisted of liquid bio-oil (55-70 wt %), a mixture gaseous products, and charcoal. The bio-oil was comprised of different molecular weight products, derived from depolymerization and fragmentation reactions of three key biomass building blocks: cellulose, hemicellulose, and lignin. Therefore, the elemental composition of bio-oil varied with different biomass feedstocks. Some physical and chemical properties of the bio-oils derived from the sawdust, rice husk, and cotton stalk powder were summarized in **Table I**. The bio-oils contain a large number of complex compounds such as hydroxyaldehydes, hydroxyketones, sugars, carboxylic acids, phenolics, and so forth, which are generally described by a chemical formula of $C_nH_mO_k{\cdot}xH_2O$. The crude biomass pyrolysis oil contain some amounts of nonvolatile materials (35-40wt.%), such as sugars and oligomeric phenolics *etc*., which are generally difficult to be reformed and easily form carbon depositions on the catalyst surface leading to the fast deactivation of catalysts. Thus, in this work, the volatile organic components of the crude bio-oil derived from the sawdust, pretreated by vapor the crude bio-oil from 80 ^{o}C to 180 ^{o}C, were used for the reforming experiments. The amount of the volatile organic components was about 50-60 wt % of the crude oil. **Table II** shows some chemical properties of crude bio-oil and the pretreated bio-oil derived from the sawdust.

Table I. The elemental compositions and characteristics of bio-oils derived from the sawdust, rice husk, and cotton stalk powder.

feedstocks	elements in bio-oil (wt%)			H_2O (wt%)	ash (wt%)	density (kg/m^3)	LHV (MJ/kg)	PH
	C	H	O					
sawdust	54.5	6.7	38.7	21.0	0.07	1300	18.20	2.1
rice husk	41.0	7.4	51.2	24.5	0.08	1150	17.16	3.2
cotton stalk	42.3	7.9	49.4	24.4	0.07	1160	17.77	3.3

Table II. Some chemical properties for the crude and pretreated bio-oils derived from the sawdust.

Composition (wt%)	crude bio-oil	pretreated bio-oil
H_2O	21.0	39.3
	elemental composition(wt%)	
C	54.5	48.5
H	6.7	8.2
O	38.7	43.3
chemical formula	$CH_{1.48}O_{0.53}{\cdot}0.32H_2O$	$CH_{2.03}O_{0.67}{\cdot}0.89H_2O$

2. Reaction system, operating procedures, analysis of products and temperature distribution

As shown in **Fig. I**, the bio-oil steam reforming experiments were carried out in the continuous flow systems, using a quartz fixed-bed reactor under atmospheric pressure. The bio-oil was fed into the reactors using the multi-syringe pump (Model: TS2-60, Baoding Longer Precision Pump), the steam from a steam-generator was simultaneously fed into the reactors for adjusting the S/C ratio (mol ratio of steam to carbon in bio-oil fed). The steam amount fed was controlled by the mass flow controller, and the effluent gases from the reactors were measured by flow display. Temperature and its distribution were measured by the thermocouples inserted into the catalyst beds. We performed the reforming experiments with following two models, *i.e.*, the common steam reforming (CSR) model and the electrochemical catalytic reforming (ECR) model. For the ECR model, an annular Ni-Cr wire, which passed through a given ac electronic current, entwined around a quartz column for heating the catalyst and synchronously providing the electrons onto the catalyst, and installed in the center of the reactor. The catalyst was uniformly embedded around the Ni-Cr wire. To make a certain reforming temperature, the catalyst bed was heated by a supplementary outside furnace or cooled via a circulation-water. For the CSR model, ac current was shut off and the catalyst bed was homogeneously heated by an outside furnace.

The products of the reforming reactions were analyzed by two on-line gas chromatographs (GC1 and GC2) with thermal conductivity detector (TCD). The products of H_2, CO and CH_4 and other hydrocarbons were detected by GC1 (Molecular Sieve 5A). The

CO_2 formed was detected by GC2 (GDX-502). The intermediates desorbed from the catalyst surface were mass analyzed by a time-of-flight (TOF) mass spectrometer. The experimental setup of the TOF system has been described in detail elsewhere [Ref.16,17]. Here, a quartz-tube reactor was installed in the center of the sample chamber of the TOF system. For the ECR model, an electrified Ni-Cr wire was embedded in the catalyst, used for heating the catalyst and providing the electrons onto the catalyst. The reactants or carrier gas (argon) were fed onto the quartz-tube reactor by a nozzle with a total pressure of about 10^{-1} Pa in the reactor tube. A small amount of the products (including intermediates formed in the reforming reactions) passed through a pinhole of about 100 μm (locating in the center of the reactor), which allows a simultaneous analysis via the TOF mass spectrometry (**Fig. 3(d)**).

The calculation methods for the hydrogen yield and carbon conversion were described in detail in our previous work [Ref.12]. Briefly, the hydrogen yield was calculated as a percentage of the stoichiometric potential, in case of complete conversion of carbon element in the bio-oil to CO_2 according to the reaction ($C_nH_mO_k$+ (2n-k) H_2O = (2n+m/2-k)H_2 + nCO_2). The potential yield of hydrogen is (2n+m/2-k) mole per mole of carbon in the feed. The carbon conversion was calculated by the total mol carbon in the gaseous products divided by the mol carbon in the fed bio-oil. Generally, all experiments were repeated three times. The difference for each repeating, in general, ranged from zero to about 10 %.

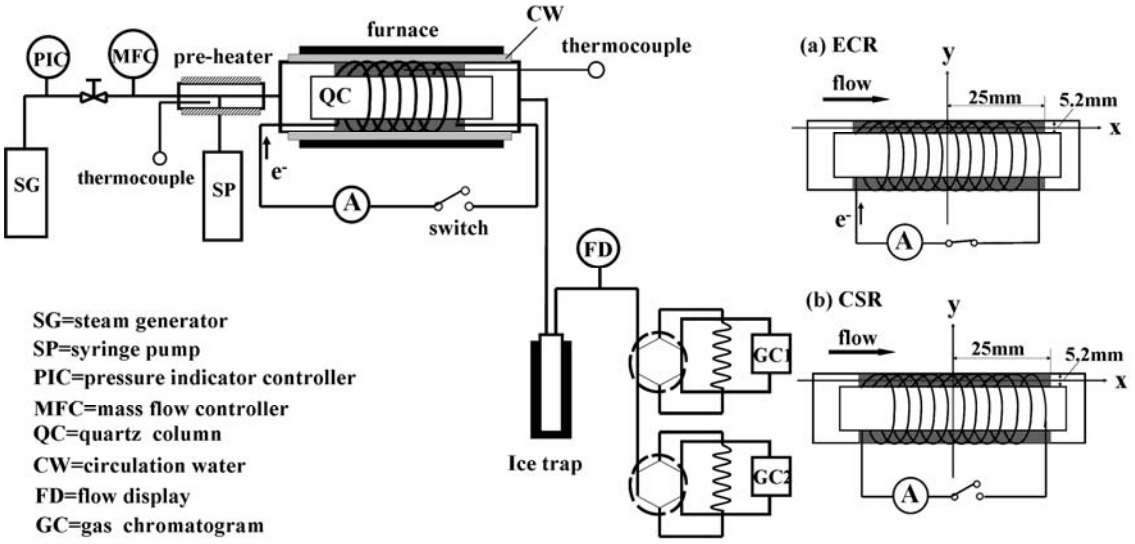

Figure I. Schematic setup of the fixed-bed flow reaction system for the bio-oil (left). Right: **(a)** ECR model: the catalyst was uniformly embedded around the Ni-Cr wire, which passed through an ac electronic current for heating the catalyst and synchronously providing the electrons onto the catalyst. **(b)** CSR model: the current was shut off and the reactor was homogeneously heated by an outside furnace.

The temperature distribution in the catalyst bed was tested before running the reforming experiments. **Table III** shows typical results of the temperature distribution for ECR and CSR. When temperature in the center of the ECR catalyst bed was near 500 ^{o}C, the maximal temperature gradients in the transverse and lognitudinal orientation were about 2 ^{o}C and 5 ^{o}C respectively for low flow speed (30 ml/min). With increasing the flow speed, both maximal temperature gradients in the transverse and lognitudinal orientation increased, reaching about 4 ^{o}C and 12 ^{o}C respectively for total flow speed of 400 ml/min. Otherwise, the temperature gradients in the CSR are slightly smaller than those in the ECR model. The center temperature, generally, is almost close to the average value (the deviations between the center temperature and the average value were less than 10 ^{o}C) in our investigated range (400-600 ^{o}C). In a convenient manner, the temperature in the center of the catalyst bed was approximately used as the reaction temperature in the ECR or CSR reforming experiments.

Table III. Temperature distribution in the catalyst bed for the ECR and CSR models.

f_{total} (ml/min)	P_{ECR} (x,y)[a]	T_{ECR}(^{o}C)	P_{CSR}(x,y)[b]	T_{CSR}(^{o}C)
30	(0, 0)	501	(0, 0)	500
	(25mm, 0)	502	(25mm, 0)	502
	(-25mm, 0)	497	(-25mm, 0)	498
	(0,1.5mm)	503	(0,1.5mm)	500
	(0,-1.5mm)	502	(0,-1.5mm)	501
400	(0, 0)	499	(0, 0)	501
	(25mm, 0)	506	(25mm, 0)	504
	(-25mm, 0)	494	(-25mm, 0)	496
	(0,1.5mm)	502	(0,1.5mm)	500
	(0,-1.5mm)	503	(0,-1.5mm)	500

[a] The coordinate in the ECR was shown in **Fig. I**. NiO/Al_2O_3 catalyst: 5.5g, total flow speed: 30 and 400 ml/min, S/C=5.8, *I*=3.8A pressure: 1.0 atm.
[b] The coordinate in the CSR was shown in **Fig. I**. The experimental conditions were same in ECR.

3. Influences of the current on the microcosmic properties of the catalyst

The Influences of current on the catalyst properties were investigated by measuring the BET surface area, pore diameter, pore volume, the level of the NiO reduction and the size of the crystallites. **Table IV** summarized the data obtained from four samples, **(a)** the fresh 18%NiO/Al_2O_3 catalyst; **(b)** the used one after the CSR of the bio-oil for 5 hours; **(c)** the used one after the ECR of the bio-oil for 5 hours; and **(d)** the treated one via a current passing though the catalyst for 10 hours under the argon ambience, respectively.

In comparison with the fresh catalyst, the BET surface area and pore volume from the used ones after CSR or ECR slightly decreased, accompanied with the increase of pore diameter and the crystallite size. After a current passed though the catalyst under the argon ambience, a bit of decrease of the BET surface area together with the increase of the crystallite size was also observed. Generally, the decrease of the BET surface area or the increase of the crystallite size will lead to the decrease of the catalyst activity. However, it was observed that the current applied in ECR obviously promoted the hydrogen production from the bio-oil**.** Based on the stability test of the catalyst during the ECR, no obvious change of the hydrogen yield was observed for the initial 5 hours **(**reforming conditions: *I*=3.0A, *T*=500 ^{o}C, *S/C*=5.8, *GHSV* =6048 h^{-1}, and *P*=1 atm**)**. The hydrogen yield gradually decreases by about 10 % (from about 91.3 % to 81.6%) for 18 h reforming, and dropped to 50% of initial value for about 35 h reforming. The catalyst deactivation mainly caused by the deposition of carbon (coke-formation) on the catalyst. The amount of the carbon deposition estimated by the TGA (Thermogravimetry Analysis) measurements was about 9.6% after the ECR of bio-oil for 35 h reforming. The above results indicate that, for the initial 5 hours, the alterations of the catalyst properties induced by the current would have a minor influence on the hydrogen production from the ECR of the bio-oil.

Table IV The Brunauer-Emmett-Teller surface area (BET *SA*), pore volume (*PV*), pore diameter (*PD*), the size of the crystallites (*d*), the level of the catalyst reduction in the catalyst body (r_b), and the level of the catalyst reduction on the catalyst surface (r_s) for the fresh catalyst and the used ones after the CSR (common steam reforming) and ECR (electrochemical catalytic reforming) for the bio-oil.

Samples	BET *SA* (m^2/g)	*PV* (cm^3/g)	*PD* (nm)	*d* (nm)[d]	r_b(%)[e]	r_s(%)[f]
fresh	115.1	0.28	9.69	$6.1_{(NiO)}$	0	0
CSR[a]	106.9	0.25	9.34	$5.4_{(Ni)}$	29.7	28.7
ECR[b]	98.7	0.27	10.92	$8.6_{(Ni)}$	52.1	50.8
Current-Ar[c]	86.8	0.26	11.92	$9.5_{(Ni)}$	100	100

[a] the used 18% NiO/Al_2O_3 catalyst after the CSR reforming of bio-oil for 5 hours (reforming conditions: *T*=500 ^{o}C, *S/C*=5.8, *GHSV* =6048 h^{-1}, and *P*=1 atm);

[b] the used 18% NiO/Al_2O_3 catalyst after the ECR reforming of bio-oil for 5 hours (reforming conditions: *I*=3.0A *T*=500 ^{o}C, *S/C*=5.8, *GHSV* =6048 h^{-1}, and *P*=1 atm);

[c] the treated 18% NiO/Al_2O_3 catalyst via a current passing though the catalyst under the argon ambience for 10 hours (treatment conditions: *I*=4.2A *T*=550 ^{o}C, *GHSV* =6048 h^{-1}, and *P(*Ar*)*=1 atm),

[d] The size of the crystallites was estimated from the peak of XRD by the Scherrer equation.

[e] The level of the catalyst reduction in the catalyst body, described by the ratio of $r_b=[Ni^0]_b$ (atomic %)/{$[Ni^0]_b$ (atomic %) +$[Ni^{2+}]_b$ (atomic %)}, was estimated from the XRD diffraction patterns and calibrated with standard spectra from Ni and NiO samples.

[f] The level of the catalyst reduction on the catalyst surface, described by the ratio of $r_s=[Ni^0]_s$ (atomic %)/{$[Ni^0]_s$ (atomic %) +$[Ni^{2+}]_s$ (atomic %)}, was estimated from the XPS spectra and calibrated with standard spectra from Ni and NiO samples.

4. Influences of the current on the level of the NiO reduction

The NiO reduction into the metallic Ni during the ECR and CSR of bio-oil were investigated by the XPS and XRD measurements. **Fig. II** shows typical Ni XPS spectra (left) and XRD spectra (right) from **(a)** the fresh 18% NiO/Al_2O_3 catalyst prepared; **(b)** the used one after CSR for 5 hours; **(c)** the used catalyst after ECR for 5 hours; and **(d)** the treated catalyst via a current passing though the catalyst under the argon ambience for 10 hours, respectively. For the Ni XPS spectrum in **Fig. II (a)**, the bind energy at about 855.4 eV and 861.9 eV were observed for the pristine catalyst, corresponding to the main line of $Ni^{2+}(2p_{3/2})$ and its satellite, respectively. After CSR, the Ni XPS spectra was similar to that of the fresh one, but an identifiable peak near 852.2 eV was observed (**Fig.II (b)**), corresponding to the metallic $Ni^0(2p_{3/2})$. This means that that Ni is nearly in +2 "formal" oxidation states in the fresh catalyst prepared. After CSR, part of Ni^{2+} on the catalyst surface was reduced to metallic Ni^0 through the surface reaction ($NiO(s) + H_2(s) \rightarrow Ni^0(s) + H_2O(s)$, here s represents the surface), where H_2 was produced by the reforming of bio-oil. On the other hand, After ECR for 5 h (**Fig. II(c)**), the $Ni^0(2p_{3/2})$ peak appeared remarkably stronger, accompanied by an obvious decrease of the main line and its satellite of $Ni^{2+}(2p_{3/2})$. The relative contents (atomic %) of the Ni element on the catalyst surface were estimated by the calibrated peak area obtained from the XPS spectra with pure Ni as a standard. **Table IV** summarized the data of the level of the catalyst reduction measured from four different samples. The level of the catalyst reduction on the catalyst surface for ECR, described by the ratio of $r=[Ni^0]_s/([Ni^0]_s+[Ni^{2+}]_s)$ was about 50.8%, which was obviously higher than the value of 28.7% for CSR. The above results showed that an additional number of $Ni^{2+}$was reduced to Ni^0 after ECR. The additional reduction of Ni^{2+} for ECR may be attributed to the surface reaction of Ni^{2+} with the thermal electrons ($Ni^{2+} + 2e^- \rightarrow Ni^0$). This explanation was supported by two facts: (1) the desorption of the thermal electrons from the electrified catalyst was directly observed by the TOF measurements (**Fig. 3** in text) and (2) the complete reduction from the oxidation state to the metallic phase was also observed when a current passed though the catalyst under the argon or helium ambience (**Fig. II(d)**).

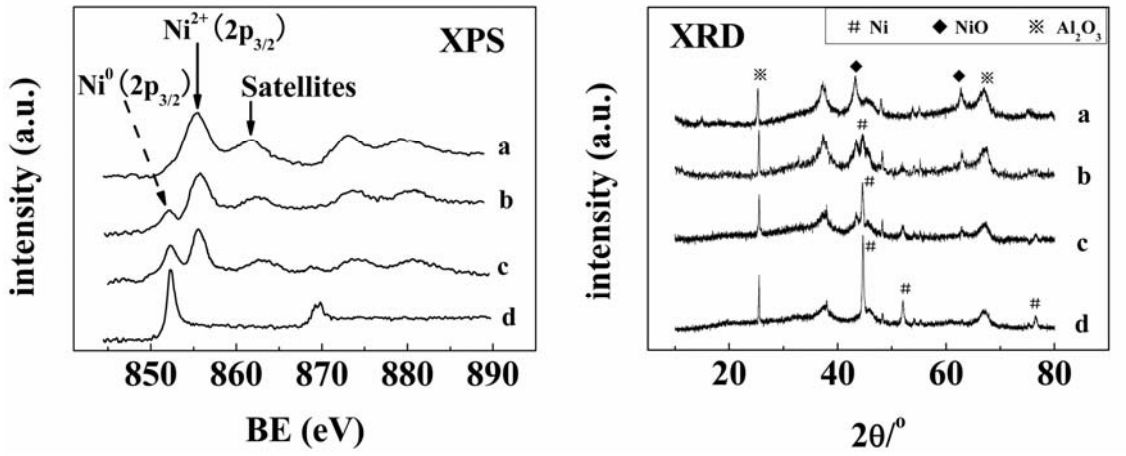

Fig. II Typical Ni XPS spectra (left) and XRD spectra (right) from **(a)** the fresh 18% NiO/Al_2O_3 catalyst; **(b)** the used 18% NiO/Al_2O_3 catalyst after the CSR reforming of bio-oil for 5 hours (other conditions :*T*=500 ^oC, *S/C*=5.8, *GHSV* =6048 h^{-1}, and *P*=1 atm); **(c)** the used 18% NiO/Al_2O_3 catalyst after the ECR reforming of bio-oil for 5 hours (other reforming conditions: *I*=3.0A, *T*=500 ^oC, *S/C*=5.8, *GHSV* =6048 h^{-1}, and *P*=1 atm); and **(d)** the treated 18% NiO/Al_2O_3 catalyst via a current passing though the catalyst under the argon ambience for 10 hours (treatment conditions: *I*=4.2A, *T*=550 ^oC, *GHSV* =6048 h^{-1}, and *P(*Ar*)*=1 atm), respectively.

Fig. II (right) shows typical XRD spectra from the four samples mentioned above. For the fresh catalyst (**Fig. II (a)),** the NiO phase (43.3 ^{o} and 62.8 ^{o}) was observed. Beside the diffraction peaks of NiO, it was also observed new peaks at $2\theta = 44.7^o$, 52.0^o and 76.5^o in **Fig. II (b)**, which were attributed to the diffraction structure of the Ni(111), Ni(200), Ni(220) phase respectively. This indicates that, after CSR, part of NiO in the catalyst body was reduced into the metallic Ni (*i.e.*, $NiO + H_2 \rightarrow Ni^0 + H_2O$). On the other hand, the XRD pattern for the used catalyst after ECR is quite different from that of the fresh one. As shown in **Fig. II(c)**, the relative intensity of the Ni diffraction peaks became remarkably strong, accompanied with the decrease of the NiO phase. This means that an additional amount of NiO was reduced into the metallic Ni during the electrochemical catalytic reforming, which is agreed with the XPS results. The reduction level in the body of the catalyst for ECR (described by the ratio of $r=[Ni^0]_b/([Ni^0]_b + [Ni^{2+}]_b)$) was about 52.1% , which was also higher than the value from CSR (29.7%, **Table IV**). Besides, the reduction from Ni^{2+} to Ni^0 was also observed from the XED spectra when a current passed though the catalyst under the argon ambience (**Fig. II (d)**). Thus, it would be concluded that the NiO phase was reduced into the metallic Ni mainly by the thermal electrons (*i.e.*, $Ni^{2+} + 2e^- \rightarrow Ni^0$), accompanied by the reduction via hydrogen (*i.e.*, $Ni^{2+} + H_2 \rightarrow Ni^0 + H_2O$) formed during the electrochemical

catalytic reforming process. In order to further make clear the promoting effects of the current on the hydrogen production, we studied the differences of the reforming between the NiO and Ni catalysts under the conditions with and without the current, as discussed below.

5. Comparison between NiO and Ni

To make clear the differences of the initial reforming performances between the NiO-Al_2O_3 and Ni-Al_2O_3 catalysts, we performed the bio-oil reforming experiments using the above two catalysts both for ECR and CSR. The Ni-Al_2O_3 catalyst was first prepared by reducing the NiO-Al_2O_3 at 650 ^oC under the flowing hydrogen ambience for 4 h, the condition is sufficient to ensure NiO reduction (as confirmed by the XPS and XRD) but not so high as to cause Ni sintering. **Fig. III** presents the yield of hydrogen (left) and the carbon conversion (right), measured as a function of temperature for **(a)** CSR (*I*=0 A) using the NiO-Al_2O_3 catalyst, **(b)** CSR (*I*=0 A) using the Ni-Al_2O_3 catalyst, **(c)** ECR (*I*=3.0 A) using the NiO-Al_2O_3 catalyst, **(d)** ECR (*I*=3.0 A) using the Ni-Al_2O_3 catalyst, respectively. Both the NiO-$Al_2O_3$and Ni-Al_2O_3 catalysts have the catalytic activity for the reforming of the bio-oil. The reforming activity over the Ni-Al_2O_3 catalyst is somewhat higher than that over the NiO-Al_2O_3 catalyst in our investigated region. For example, in the case of *I*=0 (*i.e.*, CSR), the carbon conversion over the NiO-Al_2O_3 was about 44.8 % at 500 ^oC, and reached 60.7 % over the Ni-Al_2O_3 at the same temperature. In particular, the prominent influence of the current on the carbon conversion was also observed for the Ni-Al_2O_3 catalysts. This means that the promoting effects of the current on the production of hydrogen from the bio-oil, observed in the ECR process via the NiO-Al_2O_3 catalyst, could not be mainly attributed to the reduction of NiO into Ni. More importantly, the current applied plays a significant role in promoting the decomposition and reforming of the oxygenated organic compounds ($C_nH_mO_k$) in the bio-oil, as described below. Additionally, the hydrogen yield also increased with increasing the current either over the NiO-Al_2O_3 catalyst or Ni-Al_2O_3 catalyst, as shown in **Fig. III.**

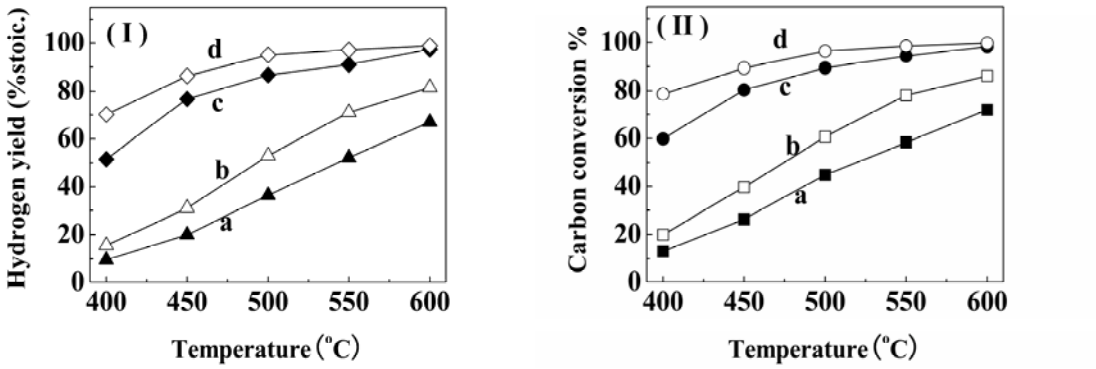

Fig. III. The yield of hydrogen (left) and the carbon conversion (right), measured as a function of temperature for **(a)** CSR (I=0 A) using the NiO-Al_2O_3 catalyst, **(b)** CSR (I=0 A) using the Ni-Al_2O_3 catalyst, **(c)** ECR (I=3.0 A) using the NiO-Al_2O_3 catalyst, **(d)** ECR (I=3.0 A) using the Ni-Al_2O_3 catalyst, respectively. Other reforming conditions were fixed at T=400, 450, 500, 550, 600 ^oC respectively, S/C=5.8, $GHSV$ =6048 h^{-1}, and P=1 atm.

6. Influences of the current on the decomposition of the oxygenated organic compounds

The influence of current on the decomposition of the oxygenated organic compounds ($C_nH_mO_k$) in the bio-oil was tested by the homogeneous experiments over a quartz bed (the quartz sand was installed in the reactor) under the conditions with and without current. It was observed that the current applied remarkably enhanced the decomposition of the oxygenated organic compounds in the bio-oil. In the case of the decomposition without current supplied (*i.e.*, I= 0A) over the quartz bed, for example, the carbon conversion was very low (about 1.5%) at 500 ^oC (other conditions: $f_{bio\text{-}oil}$=0.74 ml/min, f_{Ar}=210ml/min, and P=1 atm). With the current of 3.9A, however, the carbon conversion increased to about 17.6 % at the same temperature. The decomposition products from the bio-oil observed are complex, including H_2, CO, CO_2 and CH_4 together with a small amount of C_2H_4, C_3H_6, and C_3H_6O, *etc*.

To further make clear the decomposition processes of the oxygenated organic compounds in the bio-oil, we also carried out the homogeneous experiments using acetic acid as a model of the oxygenated organic compounds for simplifying the reaction system. **Table V** presents the influence of current on the conversion of acetic acid and the yield of hydrogen from the homogeneous decomposition of acetic acid over the quartz bed, measured as a function of current at fixed temperatures of 500 ^oC and 600 ^oC respectively. Both the carbon conversion and the hydrogen yield increased with increasing the current, indicating

that the decomposition of acetic acid was remarkably promoted by the current. The promoting effects of current on the decomposition of acetic acid observed would be explained by the decomposition of the molecule via thermal electrons. The main products from the decomposition of HAc observed are H_2, CO, CO_2 and CH_4, which would be generated through the decomposition reactions of $CH_3COOH \rightarrow 2CO + 2H_2$ and $CH_3COOH \rightarrow CO_2 + CH_4$. In addition, the promoting effects of the thermal electrons on the decomposition and the reforming of the model oxygenated organic compounds were also further directly confirmed by time-of-flight (TOF) mass spectrometry under the low-pressure (10^{-1} Pa) condition (**Fig. 3** in the text). Further work is also required to make clear the decomposition mechanism of various oxygenated organic compounds in the bio-oil, work toward this goal is in progress.

Table V Influence of current on the conversion of HAc and the yield of hydrogen from the homogeneous decomposition of acetic acid (HAc) over the quartz bed, measured as a function of current at fixed temperatures of 500 ^{o}C and 600 ^{o}C respectively. Other conditions: f(HAc)=0.96ml/min, f(Ar)=210ml/min, and *P*=1 atm.

T(^{o}C)	I (A)	Conversion of HAc (%)	Yield of hydrogen (%)
500	0	1.0	0.7
500	1	1.2	0.9
500	2	6.4	4.8
500	3	9.5	7.2
500	4	14.8	10.9
600	0	19.9	15.5
600	1	20.6	16.7
600	2	24.1	18.6
600	3	34.3	26.8
600	4	48.7	39.1

7. Mass balance and Conversion of oxygen

The composition of the products from the ECR (electrochemical catalytic reforming) of the bio-oil was dominated by hydrogen and CO_2 together with small amount of CO and trace amount of CH_4 and/or C_2H_4 *etc*.. In order to further quantitatively study the reforming product distribution, we evaluated the carbon balance, oxygen-balance and hydrogen balance in the bio-oil and acetic acid in ECR processes. The carbon balance was defined as the ratios of all carbon-containing product moles (including coke) to the consumed moles of the oxygenated organic compounds ($C_nH_mO_k$), accounting for stoichiometry. The oxygen-balance and the hydrogen balance were calculated by using similar definition as the carbon balance. **Table VI s**ummarized the results of the overall mass balance for the bio-oil and acetic acid reforming under three ECR conditions. Based on the estimation of the carbon balance and the oxygen-balance, most of the carbon or oxygen in the bio-oil was converted into CO_2 and CO. Based on the estimation of the hydrogen balance, most of the hydrogen in the bio-oil was converted into H_2 . On the other hand, it was also found that almost all of the oxygen in the acetic acid (CH_3COOH) was converted into CO_2 and CO.

Definitely, the oxygen content in bio-oil is very high. For the bio-oil used in present work, for example, the ratio of the main elemental composition (in wt %) of C, H, and O was about 48.5:8.2:43.3.Based on the analysis of the products and mass balance, most of the oxygen composition in the bio-oil is mainly converted into CO_2 and CO through the steam reforming reactions of the oxygenated organic compounds ($C_nH_mO_k$) in bio-oil ($C_nH_mO_k$ + (n-k) $H_2O \rightarrow nCO + (n + m/2 - k) H_2$), followed by the water-shift reaction ($CO + H_2O \rightarrow CO_2 + H_2$). The water is also a reactant in the production of hydrogen from the reforming of bio-oil. The modulation of the S/C ratio (mol ratio of steam to carbon in bio-oil fed) by the additive steam can promote the production of hydrogen from the bio-oil. The optimum S/C generally ranges from 4 to 7, depending on other reforming conditions setup.

Table VI The mass balance (*i.e.*, C, H, O) for the bio-oil and acetic acid reforming under three ECR conditions (T=450,500,550 ^{o}C respectively, *S/C*=5.8, *GHSV* =6048 h^{-1}, and *P*=1 atm).

	bio-oil			acetic acid		
Temperature (^{o}C)	450	500	550	450	500	550
I(A)	3.8	3.8	3.8	3.0	3.0.	3.0
% Carbon in gas-phase effluent:						
% Carbon in CO_2 product	67.8	66.5	64.8	83.7	81.0	78.4
% Carbon in CO product	23.8	30.4	34.1	13.8	17.6	23.1
% Carbon in CH_4 product	0.9	0.4	no	1.4	0.2	0.1
coke	1.8	1.2	1.9	1.2	0.7	0.5
% Carbon in liquid-phase effluent:	-	-	-			
% Carbon in liquid C_3H_6O				0.5	no	no
Carbon balance [a] (% feed)	94.3	98.5	100.8	100.6	99.5	102.1
% Oxygen in CO_2 product	81.7	80.6	79.2	91.4	90.4	88.3
% Oxygen in CO product	14.6	17.3	20.0	7.6	9.9	13.4
% Oxygen in liquid-phase effluent:	-	-	-			
% Oxygen in liquid C_3H_6O				0.09	no	no
Oxygen balance [b] (% feed)	96.3	97.9	99.2	99.1	100.3	101.7
% Hydrogen in H_2 product	94.2	98.5	99.5	98.7	99.6	101.8
% Hydrogen in CH_4 product	0.9	0.3	no	1.5	0.2	0.1
% Hydrogen in liquid-phase effluent:	-	-	-			
% Hydrogen in liquid C_3H_6O				0.3	no	no
Hydrogen balance [c] (% feed)	95.1	98.8	99.5	100.5	99.8	101.9

[a] The carbon balance: defined as the ratios of all carbon-containing products moles (including coke) to the consumed moles of the oxygenated organic compounds ($C_nH_mO_k$), accounting for stoichiometry.
[b] The oxygen balance: defined as the ratios of all oxygen -containing products moles to the consumed moles of the oxygenated organic compounds ($C_nH_mO_k$) and the consumed moles of steam, accounting for stoichiometry.
[c] The hydrogen balance: defined as the ratios of all hydrogen -containing products moles to the consumed moles of the oxygenated organic compounds ($C_nH_mO_k$) and the consumed moles of steam, accounting for stoichiometry.

8. Energy efficiency and hydrogen cost

The energy efficiency and cost for production of hydrogen from bio-oil were estimated for the following two reforming models, *i.e.*, CSR and ECR models (**Fig. I**). Energy efficiency is defined as the heating value of hydrogen divided by the energy consumed by the reforming system per kilogram of hydrogen produced. We have measured total lowest energy consumed both for CSR and ECR under the middle and higher hydrogen yield. The

consumed energy for ECR included the power of the inner and outside heaters and that for producing the steam from the steam-generator. The consumed energy for CSR included the power of the outside heaters, and that for producing the steam from the steam-generator. The amount of hydrogen formed from the reforming of bio-oil per hour was derived from the dry gaseous volume collected and the content of hydrogen in the mixtures.

Table VII shows the results of the energy efficiency and cost estimated from the selected technologies to produce hydrogen. The energy efficiency estimated from ECR ranged from 74% to 85%, the corresponding cost ranged from 53(kwh/kgH_2) to 46 (kwh/kgH_2). The energy efficiency estimated from CSR ranged from 47% to 58%. As can be seen, the energy efficiency in the ECR reforming process was higher than that in the CSR process. This may be attributed to the electrified Ni-Cr wire installed in the reactor, playing a dual role both in heating the catalyst and in providing the thermal electrons onto the catalyst at the same time. The thermal electrons can be used for promoting the dissociation and the reforming reactions of the oxygenated organic compounds in the bio-oil.

Table VII Energy efficiency and cost estimated from the selected technologies to produce hydrogen from the bio-oil.

React-type	Power (W)	Conv. (%)	H_2 yield (%)	η_{Energy} (%)[e]	Cost (kwh/kgH_2)[f]
ECR-1[a]	73.9	85.1	78.5	74	53
ECR-2[b]	83.2	98.9	96.6	85	46
CSR-1[c]	96.8	65.4	63.5	47	87
CSR-2[d]	122.4	96.7	93.4	58	71

[a] **ECR-1**: Electrochemical catalytic reforming of bio-oil under the reforming conditions: *T*=498 ^oC, *S/C*=5.8, *GHSV* =6040 h^{-1}, and *P*=1.1 atm.
[b] **ECR-2**: Electrochemical catalytic reforming of bio-oil under the reforming conditions: *T*=561 ^oC, *S/C*=5.8, *GHSV* =6270 h^{-1}, and *P*=1.2 atm.
[c] **CSR-1**: Common steam reforming of bio-oil under the reforming conditions: *T*=595 ^oC, *S/C*=5.8, *GHSV* =6510 h^{-1}, and *P*=1.2 atm.
[d] **CSR-2**: Common steam reforming of bio-oil under the reforming conditions: *T*=752 ^oC, *S/C*=5.8, *GHSV* =6960 h^{-1}, and *P*=1.2 atm.
[e] **Energy efficiency η_{Energy} (%)**: the heating value of hydrogen divided by the energy consumed by the reforming system per kilogram of hydrogen produced.
[f] **Cost (kwh/kgH_2):** the energy consumed in the reforming system per hour divided by hydrogen produced in kilogram per hour.